Research Article

Experimental Study on the Dynamic Characteristics of a New Long-Short Pile Composite Foundation under Long-Term Train Load

Zhao-rong Zhu,[1] Wei Guan [ID],[1,2] Kan Han,[1] Hong-gang Wu [ID],[1,2] Shou-quan Zhao,[1] and Xu Liu[2]

[1]*Northwest Research Institute Co., Ltd. of C.R.E.C, Lanzhou, Gansu 730000, China*
[2]*Guizhou University, Guiyang 550025, China*

Correspondence should be addressed to Wei Guan; 477743669@qq.com

Long-short pile composite foundation (PC-LSPCF) composed of part-screw pile and cement-soil compaction pile is a new railway foundation treatment method, which has been widely used in high-speed railway construction projects in China. To explore the dynamic characteristics and deformation characteristics of railway PC-LSPCF under long-term train loads, the dynamic characteristics of long piles, short piles, and soil between piles under long-term train loads are tested by an indoor dynamic model test. The dynamic amplification of pile and soil under dynamic load and the temporal and spatial distribution of peak response are analyzed, and the stress and deformation development mechanism of PC-LSPCF under cyclic loading of large-cycle trains is revealed. The results show that the neutral point of the long pile is at 1/2 of the pile length and that of the short pile is at 3/8 of the pile length. The part-screw pile has a certain absorption effect on vibration energy. The deformation of a long-short pile composite foundation under long-term train loads can be divided into three stages: extreme growth, transition, and stability. The train speed is negatively correlated with the cumulative settlement of the long-short pile composite foundation. The higher the train speed, the smaller the cumulative settlement, and the smaller the number of cycles of the N-S curve entering the gentle period. As the number of train cyclic loads increases, the load-sharing relationship of the long pile-short pile-soil system will be redistributed. The research results have important reference significance for the optimization design of high-speed railway foundation treatment.

1. Introduction

Since the opening of the Tokaido Shinkansen high-speed railway system in 1964, many countries have begun to vigorously develop high-speed railways. Especially in China, the current high-speed rail mileage in the world's first, high-speed rail has become one of the important means of transportation. Because the operation of high-speed trains has very strict requirements on track smoothness and postconstruction settlement of subgrade, long-short pile composite foundation (LSPCF) has been widely used in high-speed railway construction due to its high bearing capacity, small settlement, and economic rationality [1]. In recent years, a new type of long-short pile composite foundation (PC-LSPCF) composed of part-screw piles and cement-soil compaction piles has been applied to China's high-speed railway construction projects. Although several studies have shown that PC-LSPCF has good bearing capacity under static load conditions [2–4], there are few reports on the dynamic characteristics of PC-LSPCF, especially considering that the speed of high-speed railway trains has been constantly refreshed in recent years and the influence of vibration load generated during train operation on the foundation has become more and more prominent [5–7]. Whether PC-LSPCF can meet the long-term bearing requirements of the high-speed railway is still a problem.

The design concept of a long-short pile composite foundation was proposed by Chinese scholar Ma Ji in the early 21st century [8]. It forms a vertical variable stiffness composite foundation by optimizing the combination of a longer rigid pile and shorter flexible pile, which just adapts to the stress field that the additional stress of the foundation decreases with depth, and achieves the purpose of controlling uneven settlement, as shown in Figure 1. Long-short pile composite foundation has attracted wide attention in academia. Scholars in Gong's team have carried out a series of engineering practice research projects on it and elaborated and introduced its theory and practice methods [9–11]. Under the condition of static load, Zhao et al. [12] proposed a settlement calculation method for long-short pile composite foundations considering the interaction of the pile-soil-cushion system. Qian and Zhang and Guo et al. [13, 14] showed that the influence of a long pile on the overall settlement is greater than that of a short pile by different research methods. Based on the shear displacement method, Liu et al. [15] studied the influence of pile spacing on long-short pile composite foundation by the centrifugal model test and numerical simulation and put forward a reasonable range of pile spacing. Yang and Zhang [16] used finite element analysis, a field test, and the standard formula calculation method to analyze the influence of cushion thickness, pile length, and raft thickness on the axial force and side friction resistance of long piles. Under the condition of a dynamic load, Jihui et al. [17] used the finite element analysis method to analyze the displacement and acceleration time-history curve of a rigid-flexible composite foundation under blasting load. Fattah et al. [18] studied the effect of soil saturation on load transfer from a single pile under vertical vibration. Yiguo et al. [19] compared the bearing capacity of long and short pile composite foundations with and without geogrid through the model test. The results show that the relationship between the settlement of a long-short pile composite foundation and the number of cycles can be expressed by an exponential function, and the long-short pile in a composite foundation with geogrid should be greatly changed.

At present, most scholars have carried out relevant research on the static bearing capacity of long-short pile composite foundations, but there are few studies on the dynamic characteristics of long-short pile composite foundations. The existing design and calculation methods of railway long-short pile composite foundations still do not fully consider the influence of train dynamic action. Therefore, it is necessary to study the vibration response of a new long-short pile composite foundation. Therefore, through the indoor model test of PC-LSPCF under simulated train load, the characteristics of acceleration, dynamic stress, and cumulative settlement of the long pile-short pile-soil system under long-term train load are tested. The dynamic amplification of pile and soil under dynamic load and the temporal and spatial distribution of peak response are analyzed, and the development mechanism of stress and deformation of a long-short pile composite foundation under a large-cycle train cyclic load is revealed.
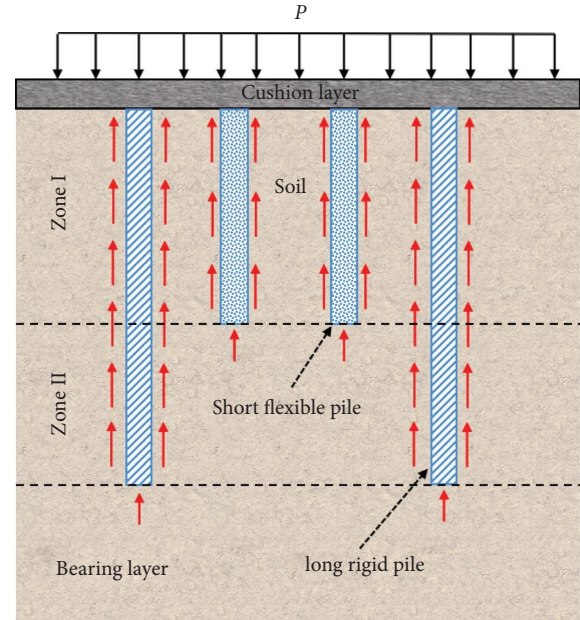

Figure 1: The schematic diagram of the long-short pile composite foundation.

2. Physical Model Experimental Design

2.1. Model Similarity Design. This test is based on a new railway roadbed treatment project in Northwest China. The subgrade of this section is treated by PC-LSPCF, in which the long pile is a part-screw pile and the short pile is a cement soil compaction pile. The length of the part-screw pile is 6.5 m, and the pile diameter is 0.4 m. The length of the cement soil compaction pile is 4 m, and the pile diameter is 0.4 m. The piles are arranged in a square pattern with the long and short piles spaced apart and the long piles spaced twice as far apart as the short piles, as shown in Figure 2. The scale test was carried out by using 4 long piles and 4 short piles. The geometric similarity ratio between the prototype and the model was 10 : 1. The foundation soil and cushion are made of undistorted materials. The material properties of prefabricated model piles are similar to those of the prototype, so the elastic modulus similarity ratio and density similarity ratio are 1 : 1. That is, $c_l = 10$, $c_E = 1$, and $c_\rho = 1$, the similarity constants of other physical quantities can be derived by Buckingham π theorem, as shown in Table 1.

2.2. Material Properties. According to the geological conditions of the prototype foundation, the soil type of the pile side is mainly the Quaternary Pleistocene alluvial silty clay, silt, sandy loess, sand, or gravel soil, and the pile end is the fine sand bearing layer. Considering the constraints of a small geometric size in a model test, the excessive stratification of model soil will increase the difficulty of revealing the mechanism [20]. Therefore, the soil is divided into two layers from the top of the pile: (1) 200 mm thick silty clay; (2) 700 mm thick fine sand (the bearing layer). Cushion material and foundation soil are both original materials. Before filling the model, the density and moisture content

of the soil were tested by the ring tool method and the drying method, the compression modulus of the soil was tested by the indoor compression test, and the permeability coefficient of the soil was obtained by the indoor seepage test. The specific parameters are shown in Table 2. When the foundation soil is filled, it is filled in layers of 5 cm and compacted layer by layer to make its density meet the design requirements. Unweathered gravel with good gradation and maximum particle size less than 50 mm is used as cushion.

The part-screw pile is simulated by gypsum material. The concrete strength grade is C25, and the pile length is 650 mm. The pile length of the straight rod section is 200 mm, and the pile length of the screw section is 450 mm. Straight rod section pile diameter is 40 mm, and screw section diameter is 30 mm. The cement soil compaction pile is simulated by using the PVC pipe with 8% cement improving the soil. The pile length is 400 mm, and the pile diameter is 40 mm. The prefabricated model pile and foundation soil materials are shown in Figure 3.

2.3. Test Equipment and Sensor Layout.

According to similar conditions, the model box is assembled by assembling steel blocks, and the size is length × width × height = 1 m × 1 m × 1 m. The test loading system consists of a vibration exciter, controller, load input control machine, and hydraulic system. The maximum test force of the exciter equipment is 500 kN, and the output action frequency range is 0~30 Hz. The controller is produced by MOOG company in Germany. Different vibration waveforms can be set according to the axle load and running speed of different trains to simulate the cyclic action of train loads.

According to the dynamic response characteristics of piles and soil between piles, the acceleration, dynamic soil pressure, and dynamic strain response characteristics of the pile-soil system were monitored. The acceleration test element is a three-way capacitive acceleration sensor. The range is ±5 g, the frequency range is 0~900 Hz, and the sensitivity is between 184.85 mV/g and 191.77 mV/g. The fixed acceleration sensor is pasted on the long pile and the short pile to test the dynamic response of the pile, and the acceleration sensor is embedded in the soil between the long pile and the short pile to test the dynamic characteristics of the soil. The dynamic Earth pressure test element is a CY200 digital pressure sensor with a measuring range of 0~100 MPa. The dynamic Earth pressure box is arranged at a certain distance along the depth direction between the long pile and the short pile to monitor the soil stress change. The dynamic strain test element is BE120-10AA-P150 resistance strain gauge, the resistance value is 120 Ω, and the sensitivity coefficient is 2.21; we select a long pile and adjacent short pile along the pile spacing paste dynamic strain gauge to monitor pile deformation characteristics. Because temperature has a great influence on the resistance strain gauge sensor, the corresponding temperature compensation sensor is connected to each test strain sensor. The acceleration signal and dynamic strain signal are collected by the DHDAS dynamic signal acquisition and analysis system, and the dynamic Earth

pressure signal is collected by the TST-PFM4.10 dynamic signal continuous monitoring system. The specific location of the sensor is shown in Figure 4.

2.4. Test Loading Programme.

Train load is an instantaneous load related to train structure, track, and speed [21]. Al Shaer et al. [22] pointed out that a single wheel load can be considered a train load, while a dynamic load is likely to be a cyclic sine wave load from a theoretical point of view. Therefore, this study uses sinusoidal cyclic load to simulate train load, which can reflect cyclic characteristics, speed effect, and geometric irregularity. The load expression is as follows:

$$P(t) = P_0 + P_a \sin(\omega t), \qquad (1)$$

where $P(t)$ is the dynamic train loads acting on top of the model foundation, unit: kN. P_0 is the constant load acting on the top of the model foundation. P_a is the half amplitude of a sine wave. $\omega = 2\pi f$ is the angular velocity, unit: rad/s. f is the loading frequency, unit: Hz. t is the loading time, unit: s.

The train load frequency can be expressed in terms of travel speed and axle spacing between wheel pairs, and the test load frequency can be calculated from the following equation:

$$f_m = c_t f_p = c_t \frac{v}{L}, \qquad (2)$$

where f_m is the test load frequency, unit: Hz; f_p is the actual load frequency, unit: Hz; c_t is the time similarity ratio; v is train speed, unit: m/s; L is the wheel-to-wheel spacing, unit: m (this experimental model takes 2.5 m).

This test is based on the Chinese CRTS-I-type slab ballastless track. The design axle load of the train is generally 200 kN. The track slab and foundation are considered to bear the design dynamic axle load of 300 kN. Therefore, the current high-speed railway subgrade structure should meet the design requirements of structural performance at a level of 300 kN dynamic axle load. According to Buckingham's π law, it can be calculated that the test dead load P_0 in this paper is 3 kN. According to the design experience of ordinary railways, the ratio of train live load to dead load is 0.2 to 0.4 [23], which is 0.33 in this test, and the value of train live load is 1 kN, that is, $2P_a = 1$ kN, $P_a = 0.5$ kN, that is, the wave load varies cyclically in the range of 2.5 to 3.5 kN.

The model test is divided into 8 test conditions to simulate the long-term vibration load generated by different train speeds. The number of excitations in each condition is 20,000 times. The test excitation frequency of train load under each condition can be calculated using formula (2). The specific loading conditions are shown in Table 3.

3. Analysis of Test Results

3.1. Time Domain Characteristics of Acceleration Response of the Long Pile-Short Pile-Soil System.

Taking the train speed of 240 km/h as an example, the vibration acceleration time history of different spatial positions of pile body and soil between piles measured by the test is shown in Figure 5. The
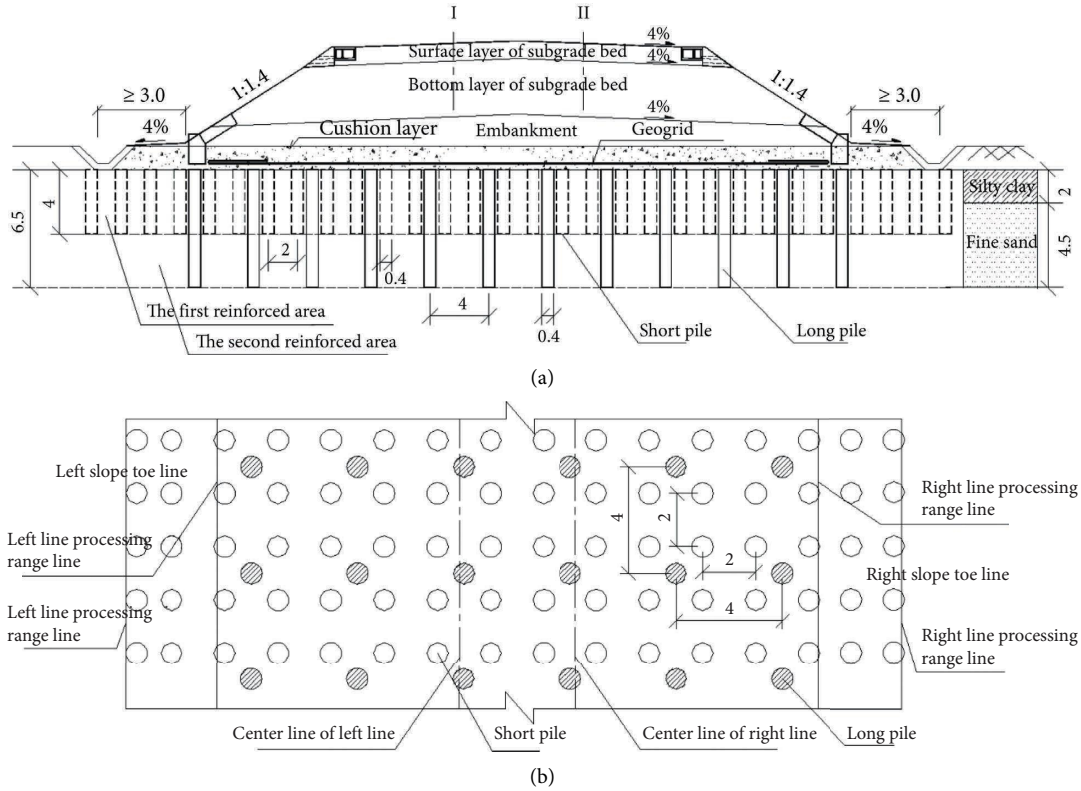
(a)

(b)

FIGURE 2: Design drawing of prototype long-short pile composite foundation treatment (unit: m). (a) Cross section of long-short pile composite foundation treatment. (b) Long-short pile composite foundation treatment plan.

TABLE 1: Similarity relation and similarity constant.

Physical quantity		Similarity relationship	Similarity ratio	Note
Geometric characteristics	Length l	C_l	10 : 1	Controlled quantity
	Area A	$C_A = C_l^2$	100 : 1	
	Displacement u	$C_u = C_l$	10 : 1	
Material characteristics	Strain ε	$C_\varepsilon = 1.0$	1 : 1	
	Stress σ	$C_\sigma = C_E$	1 : 1	
	Elastic modulus E	C_E	1 : 1	Controlled quantity
	Poisson's ratio μ	$C_\mu = 1.0$	1 : 1	
	Density ρ	C_ρ	1 : 1	Controlled quantity
	Cohesion c	$C_c = C_E$	1 : 1	
	Internal friction angle φ	$C_\varphi = 1.0$	1 : 1	
Load	Concentrated force F	$C_F = C_l^2 C_E$	100 : 1	
	Surface load q	$C_q = C_E$	1 : 1	
Dynamic characteristics	Quality m	$C_m = C_l^3 C_\rho$	1000 : 1	
	Time t	$C_t = C_l C_\rho^{0.5} C_E^{-0.5}$	10 : 1	
	Frequency ω	$C_\omega = C_t^{-1}$	0.1 : 1	
	Speed v	$C_v = C_l C_t^{-1}$	1 : 1	
	Acceleration a	$C_a = C_l C_t^{-2}$	0.1 : 1	

left side is the acceleration time history curve of the whole load cycle, and the right side is the acceleration time history enlarged view of a certain cycle. It can be seen from the figure that the acceleration response trends of long piles, short piles, and soil in the whole load cycle are synchronized, and the acceleration amplitude changes little with time. It can be seen from the enlarged view that the response form is a simple harmonic vibration. The

acceleration response amplitude of surface soil and pile top of a composite foundation is larger, in which short pile top (PS1) < long pile top (PL1) < surface soil between piles (SA1), and the peak acceleration response is 0.117 m/s², 0.126 m/s², and 0.132 m/s², respectively.

Figure 6 shows the response peak changes of long piles, short piles, and soil between piles at different positions. It can be seen that the peak acceleration response of the

TABLE 2: Test material parameters.

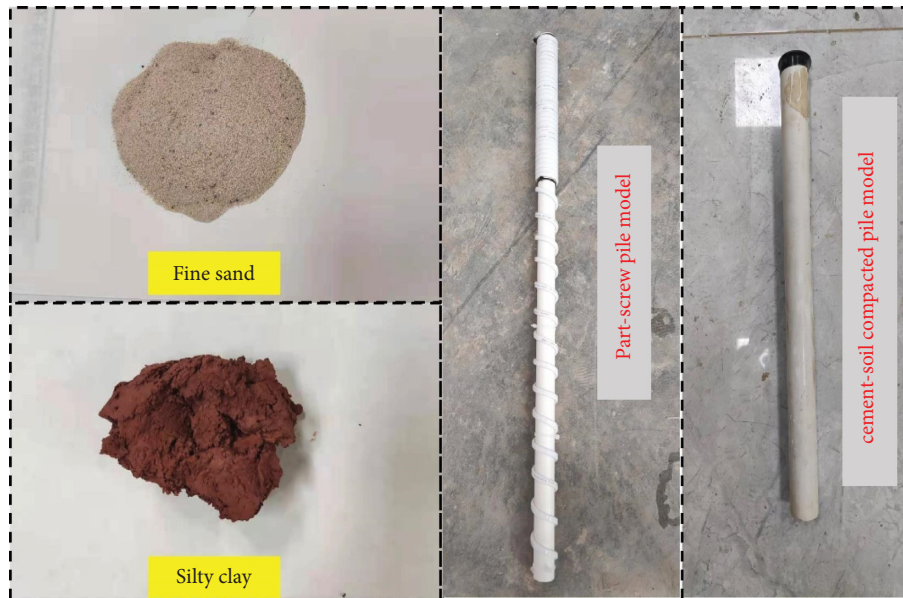| Similar materials	Density (g/cm³)	Natural moisture content (%)	Compression modulus (MPa)	Permeability coefficient (cm/s)
Silty clay	1.88	28.5	7.24	5.24×10^{-6}
Fine sand	1.73	19.7	23.67	3.59×10^{-2}

FIGURE 3: Model test material.

composite pile composite foundation at different spatial positions increases with the increase in train speed. With the increase of foundation depth, the acceleration amplitude of pile and soil has obvious attenuation. Under the conditions of low speed 160 km/h, fast 240 km/h, and high speed 360 km/h, the acceleration amplitude of the short pile bottom relative to the pile top in the first reinforcement area is attenuated by 17.97%, 23.55%, and 27.79%. The acceleration amplitude of the long pile in the second reinforced area decreased by 29.33%, 38.62%, and 44.85%, respectively, relative to the pile top. The bottom of the soil between piles decreased by 42.72%, 46.73%, and 49.81%, respectively, compared with the top soil. It shows that the faster the train runs, the greater the attenuation rate of acceleration response with the depth of foundation, and the attenuation rate of soil is greater than that of the pile.

3.2. Time Domain Characteristics of Dynamic Stress Response of Soil between Piles. Under the condition of 240 km/h, the dynamic stress time history of soil between piles at different depths obtained by the test is shown in Figure 7. The left side is the dynamic stress time history curve of the whole load cycle, and the right side is the dynamic stress time history enlarged view of a certain cycle. It can be seen from the left figure that the dynamic stress of the soil begins to increase during the initial loading period and then stabilizes at a simple harmonic wave on a certain baseline. The dynamic stress amplitude of the soil on the surface (DS1), middle (DS3), and bottom (DS5) of the pile-soil composite reinforcement area is 1.6 kPa, 3.0 kPa, and 2.5 kPa, respectively.

Figure 8 shows the distribution characteristics of the dynamic stress amplitude of soil between piles under different velocity conditions. It can be seen that the dynamic stress response in the middle of the pile-soil composite reinforcement layer is the largest, the dynamic stress response at the surface and bottom is small, and the overall distribution is an inverted "M" shape. The amplitude of the dynamic stress response of the soil between piles increases with the increase in train speed. Compared with the low-speed 160 km/h condition, the dynamic stress amplitude of the surface, middle, and bottom of the pile-soil composite reinforcement layer increased by 162.5%, 236.4%, and 240.1%, respectively, under the condition of high speed 320 km/h, indicating that the dynamic stress of the surface soil of the long-short pile composite foundation is less sensitive to the change in train speed. With the increase in foundation depth, the influence of train speed on soil dynamic stress increases.

3.3. Time Domain Characteristics of Dynamic Strain Response of the Pile. In order to understand the deformation characteristics of the pile under cyclic dynamic load, the dynamic strain test signals of the pile top measuring point, the pile middle measuring point, and the pile bottom measuring point of the long pile and the short pile are selected, respectively. The time history change under the condition of
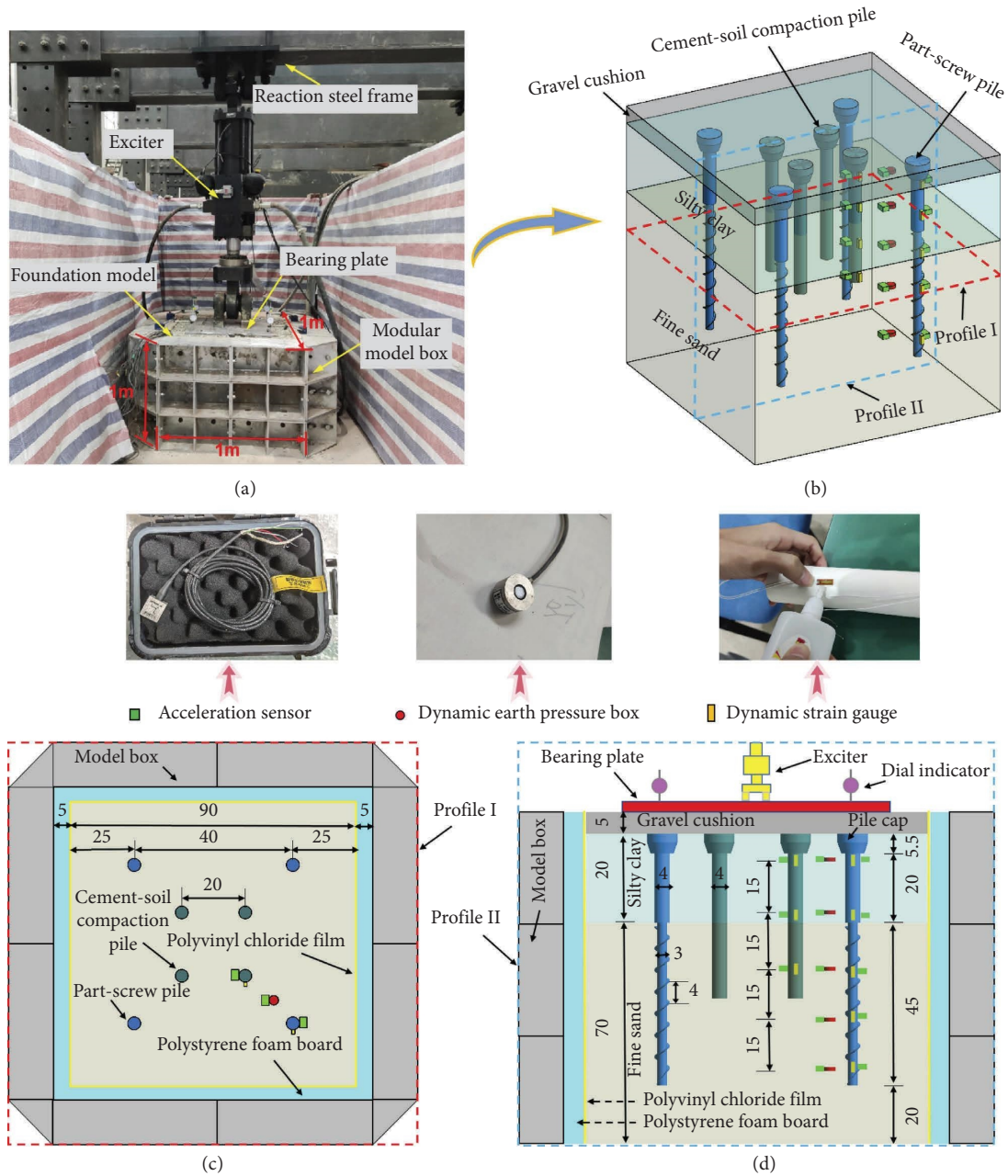
FIGURE 4: The schematic diagram of the model test design. (a) The main device of the model test. (b) The long-short pile composite foundation model. (c) Model plane diagram. (d) Model elevation diagram (unit: cm).

TABLE 3: Test loading condition.

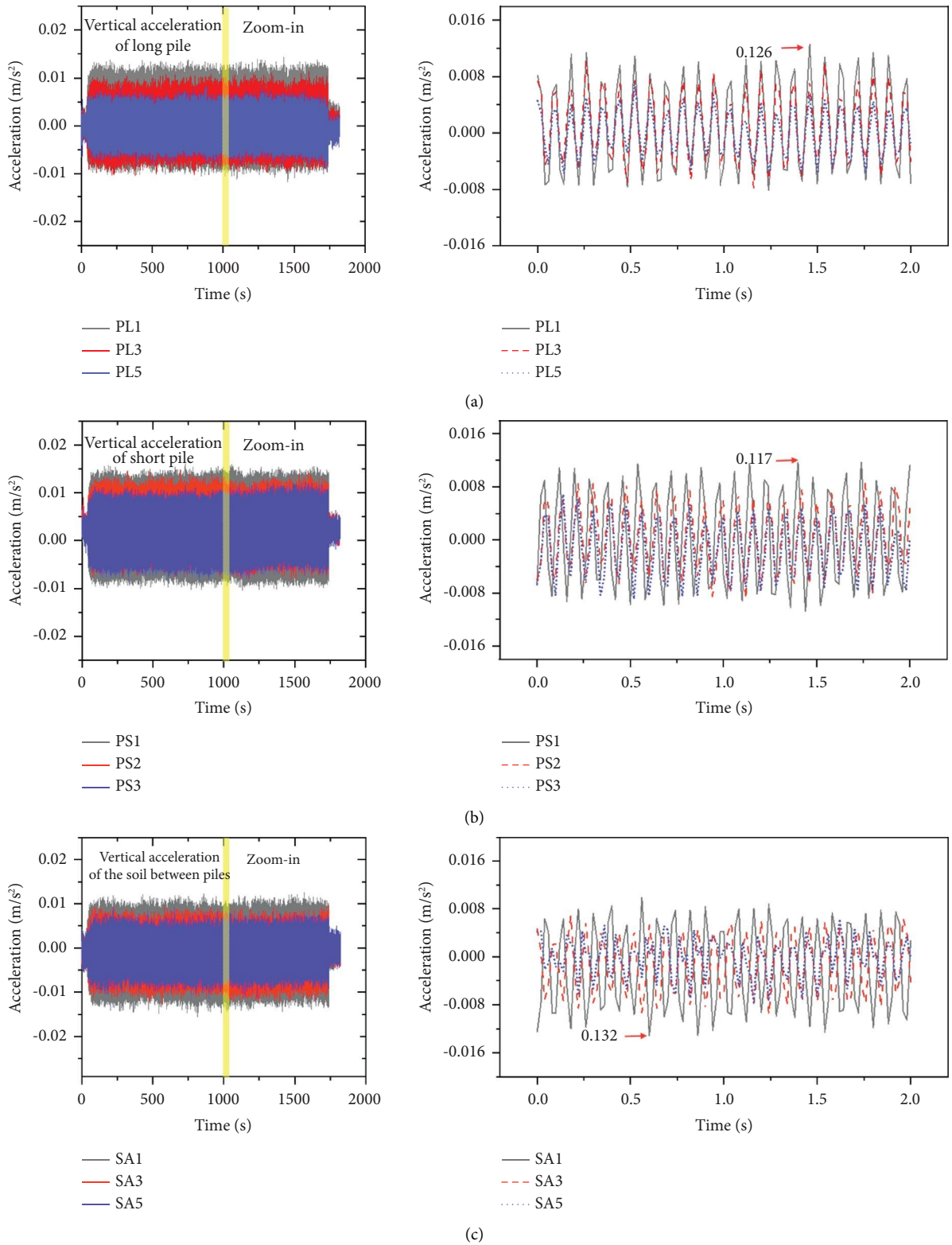| Cases	Dead load P_0 (kN)	Amplitude P_a (kN)	Frequency f (Hz)	Simulated train speed v (km/h)	Cycles
1	3	0.5	3.904	80	2×10^4
2	3	0.5	5.856	120	2×10^4
3	3	0.5	7.808	160	2×10^4
4	3	0.5	9.760	200	2×10^4
5	3	0.5	11.712	240	2×10^4
6	3	0.5	13.664	280	2×10^4
7	3	0.5	15.616	320	2×10^4
8	3	0.5	17.568	360	2×10^4

FIGURE 5: Time-history response curve of acceleration. (a) Time domain curve of acceleration response of long pile. (b) Time-domain curve of acceleration response of short pile. (c) Time-domain curve of the acceleration response of soil between piles.

240 km/h speed is shown in Figure 9. The left side is the dynamic stress time history curve of the whole load cycle, and the right side is the dynamic strain time history enlarged view

of a certain cycle. It can be seen from the left figure that the long pile and the short pile have different degrees of compression deformation at different positions. The deformation
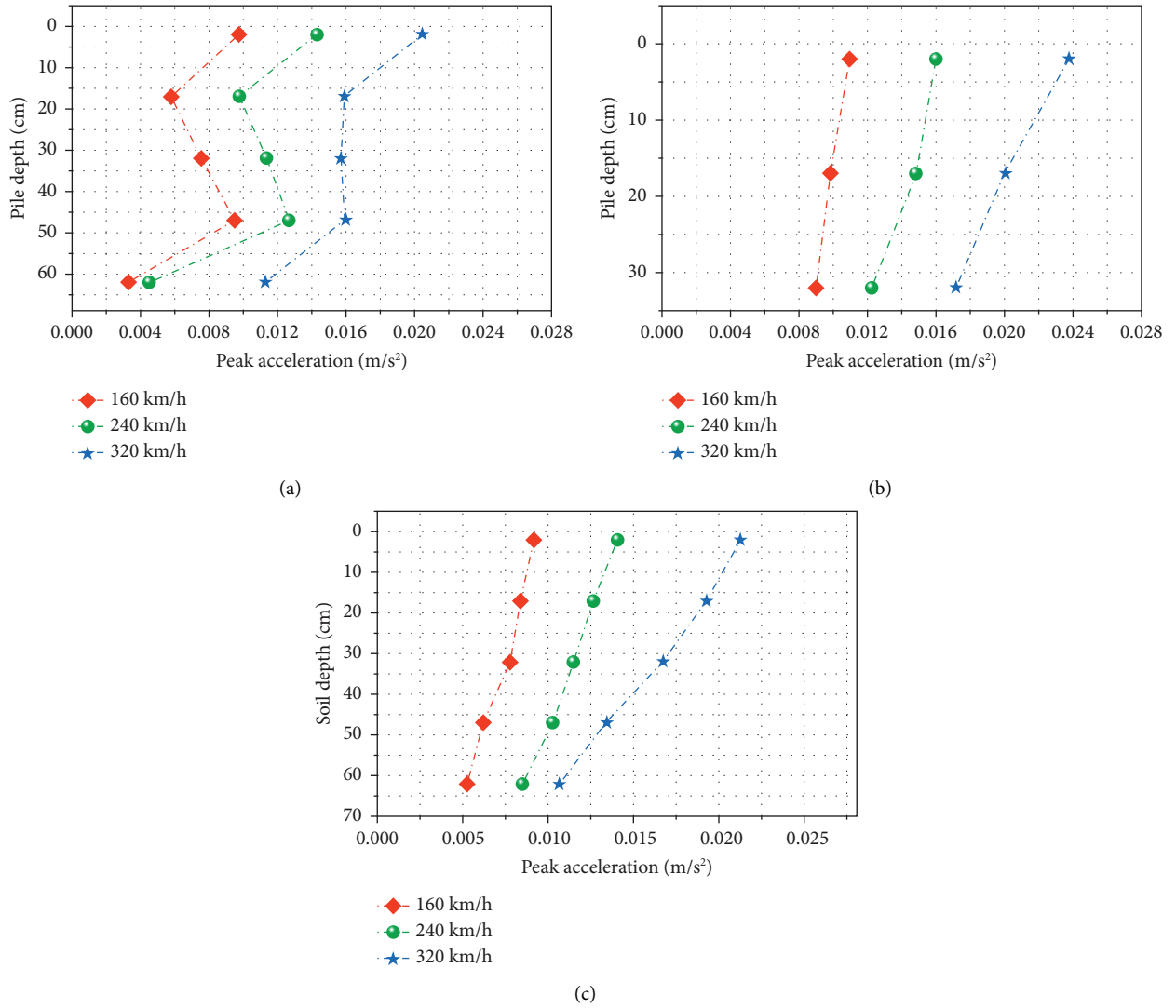
(a)

(b)

(c)

FIGURE 6: Peak distribution curve of acceleration response. (a) Peak acceleration response distribution of long piles. (b) Peak acceleration response distribution of short piles. (c) Peak acceleration response distribution of soil between piles.

increases rapidly in the initial cycle period and then stabilizes at a certain interval value. It can be seen from the enlarged view on the right that the average dynamic strain S_{AV} of the long pile at YL1, YL3, and YL5 is $-189.05 \, \mu\varepsilon$, $-866.02 \, \mu\varepsilon$, and $-52.58 \, \mu\varepsilon$, respectively. Peak-to-peak S_{PPV} was $33.35 \, \mu\varepsilon$, $111.38 \, \mu\varepsilon$, and $13.36 \, \mu\varepsilon$, respectively. The average dynamic strain S_{AV} of the short pile at YS1, YS2, and YS3 is $-227.01 \, \mu\varepsilon$, $-259.64 \, \mu\varepsilon$, and $-126.52 \, \mu\varepsilon$, respectively. The peak-peak S_{PPV} was $56.87 \, \mu\varepsilon$, $70.85 \, \mu\varepsilon$, and $33.42 \, \mu\varepsilon$, respectively. It shows that under the train vibration load, the deformation in the middle of the long pile and the short pile is the largest, especially the peak value of dynamic strain in the middle of the long pile, which is 3–5 times that of other positions and should be considered in the composite foundation of the railway composite pile.

According to the average dynamic strain S_{AV} value of different parts of the pile shaft, the axial force distribution of the pile shaft can be obtained by Hooke's law and the section method. The calculation formula is as follows:

$$F_{pi} = EA_i\varepsilon_{AV}, \tag{3}$$

where F_{pi} is the average dynamic axial force of section i of the pile. E is the elastic modulus of the pile. A_i is the area of section i of the pile. ε_{AV} is the average dynamic strain of section i of the pile.

The axial force distribution of long and short piles under different speed conditions can be obtained. It can be seen from Figure 10 that, for long piles, the axial force of the pile increases with the increase in depth within a range of 3.2 m from the top of the pile. This is because the settlement of the pile in the depth range of 0–3.2 m of the composite foundation is less than the settlement of the soil around the pile, resulting in a downward relative force, which in turn produces a negative friction resistance on the pile side, making the axial force of the pile gradually increase. In the range of 3.2∼6.2 m downward from the top of the pile, the axial force of the pile gradually decreases with the increase in depth. At 6.2 m of the pile, the axial force of the pile decreases to about
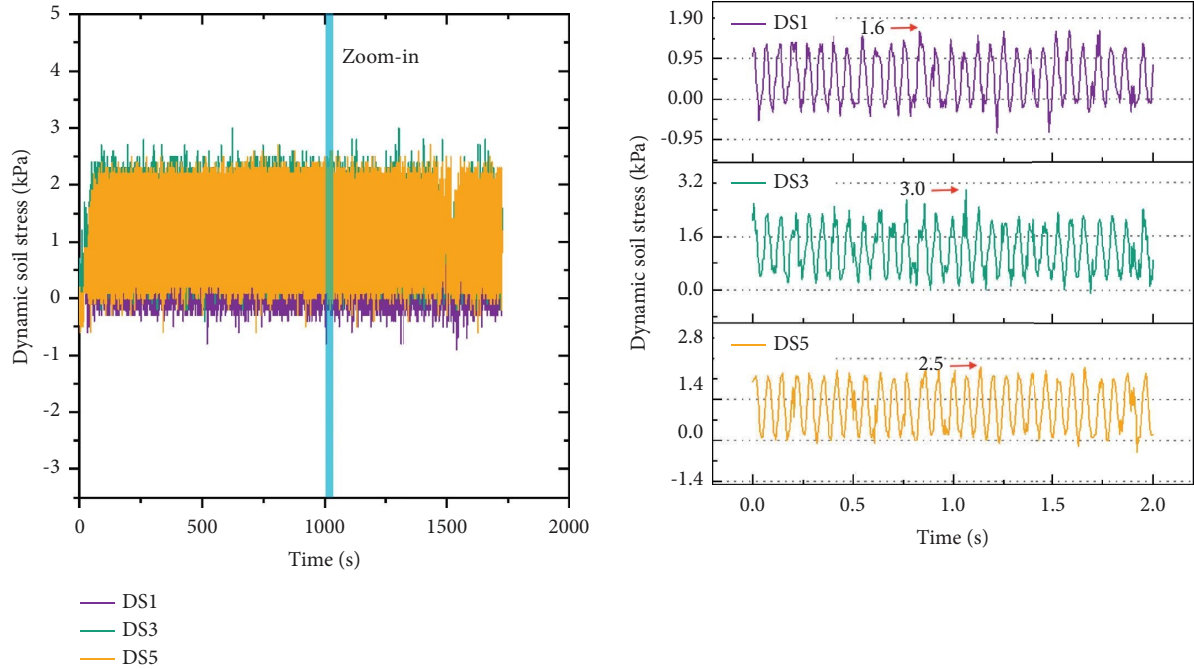
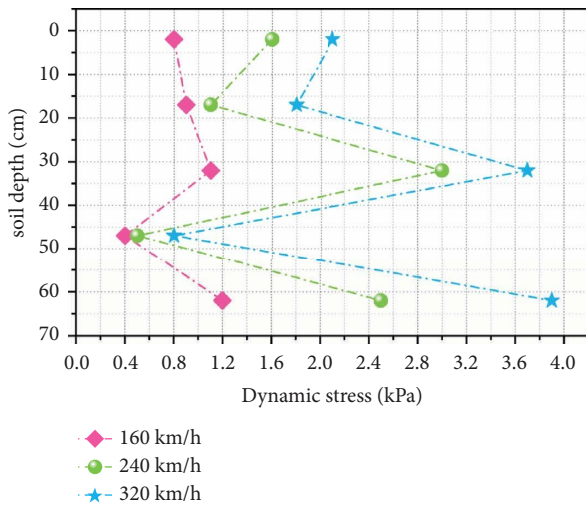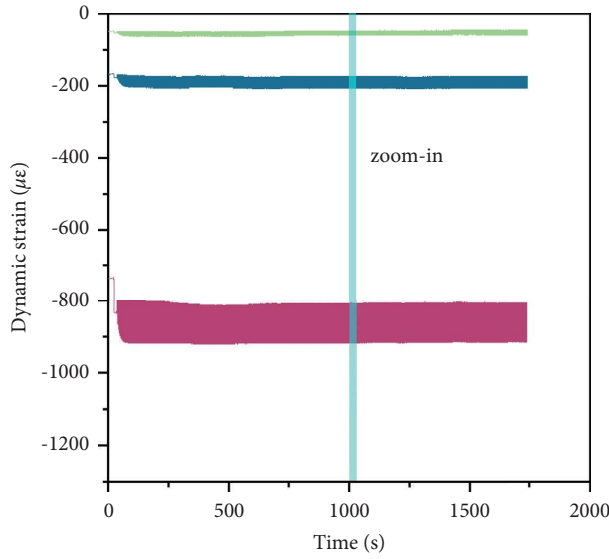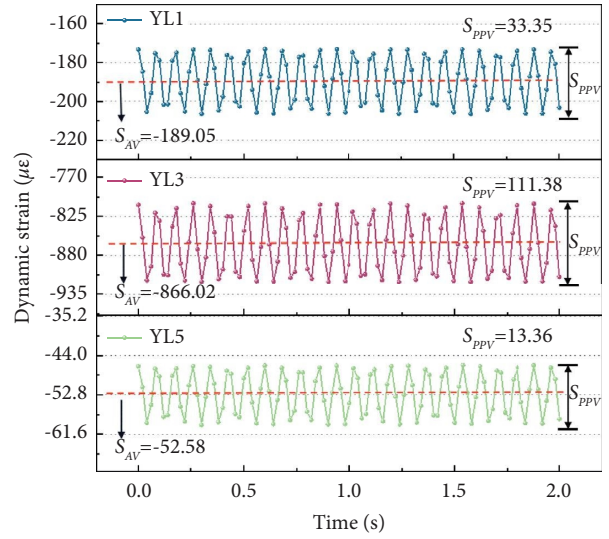FIGURE 7: The time-history response curve of dynamic soil pressure.

FIGURE 8: The peak distribution curve of dynamic soil pressure.

2.8 N. This is due to the fact that the dynamic load continuously overcomes the side friction resistance and diffuses into the soil through the side friction resistance during the downward transmission of the pile, resulting in the axial force of the pile gradually decreasing along the depth in this range [24]. Similar to the change law of long pile axial force, the axial force of the short pile increases linearly with the increase of depth in the depth of 0–1.5 m and decreases gradually with the increase of depth in the depth of 1.5–3.8 m. In summary, the axial force of the long pile reaches its maximum at 1/2 of the pile length, and the pile side friction is 0, which is the neutral point position; the axial force of the short pile reaches its maximum at 3/8 of the pile length, and the pile side friction resistance is 0, which is the neutral point position.

3.4. Dynamic Load Magnification Factor of the Pile-Soil System.
Taking the amplitude of dynamic strain (dynamic stress) at the initial stage of dynamic loading (i.e., static loading) as the reference, the dynamic load magnification factor under each frequency is the ratio of the amplitude of dynamic strain (dynamic stress) under this frequency to the amplitude of strain (stress) under static loading [25]. The measuring points YL1, YS1, and DS1 at pile top are selected as the research object, and the relationship curve between the dynamic load magnification factor Φ_d and the excitation frequency f is shown in Figure 11. According to Figure 11, the dynamic load magnification factor of the long pile, short pile, and surrounding soil varies with the excitation frequency in the same way. When the excitation frequency is less than 12 Hz, the dynamic load magnification factor increases slowly with the increase of the excitation frequency. Then, the dynamic load magnification factor increases sharply within the frequency range of 14–16 Hz, reaching a maximum of 1.8, and finally drops to a lower level around 18 Hz. In addition, under the same load frequency, the dynamic load magnification factor shows the following pattern: short pile > long pile > surrounding soil. This indicates that the resonance frequency of the long-short pile composite foundation system under train load is in the range of 14–16 Hz and that the sensitivity of the pile to dynamic load is greater than that of the surrounding soil. When the running speed is 320 km/h (load frequency 15.616 Hz), the maximum dynamic load magnification factor of the composite foundation with long and short piles obtained in this paper is 1.8, which is far less than the dynamic load magnification factor of 3.0 in the design specification of the China high-speed railway [26].
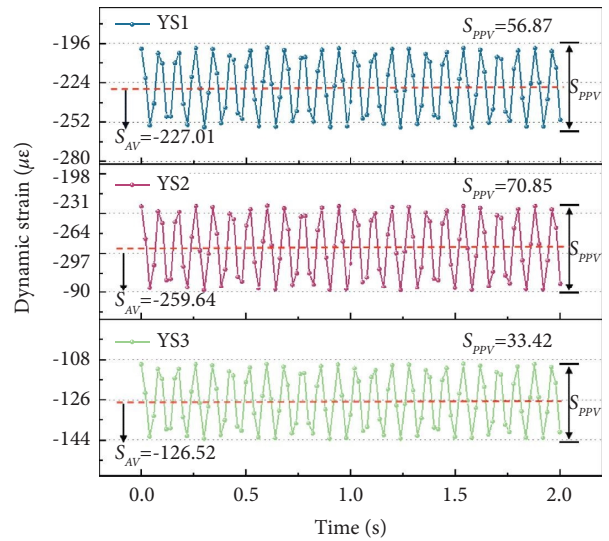
(a)
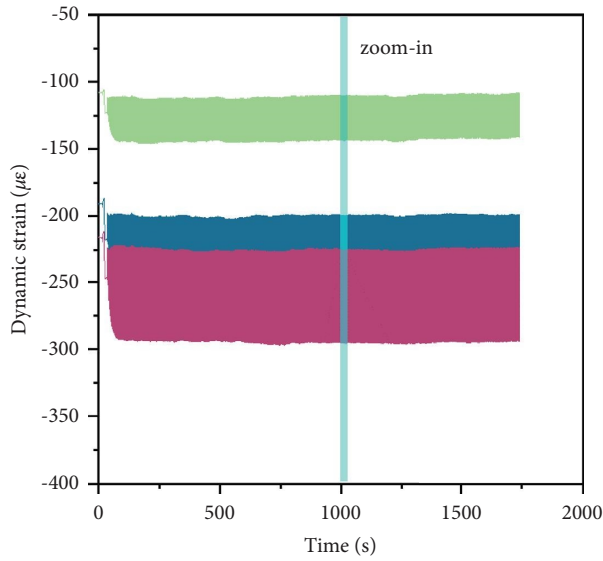
(b)

FIGURE 9: The time-history response curve of dynamic strain. (a) Time history curve of dynamic strain of the long pile. (b) Time history curve of dynamic strain of the short pile.

3.5. Variation of Long-Term Settlement of Composite Foundation.

The postconstruction settlement of the subgrade is closely related to the service performance of the railway track, and it is of great engineering significance to study the surface settlement characteristics of a composite foundation [27]. Figure 12 shows the number of cycles-cumulative settlement (N-S) scatter distribution of composite pile composite foundation under different speed conditions. It can be seen from the diagram that the settlement of the composite foundation increases with the increase in the number of cyclic loading cycles. In the early stages of cyclic loading, the settlement development rate of composite foundation is faster, but the rate of settlement increase of composite foundations decreases with the increase of cycle times. When the cycle times are large enough, the trend of the cycle times-settlement curve tends to be gentle, and the settlement development of a composite foundation is basically stable. Comparing the settlement law
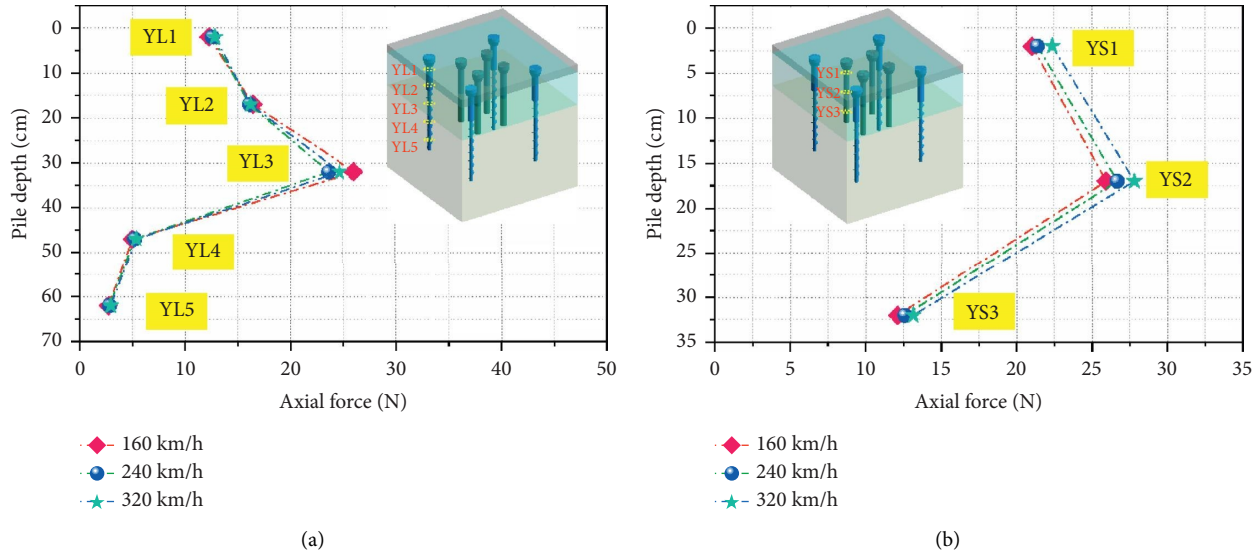
FIGURE 10: The peak distribution curve of the axial force. (a) Distribution of peak axial force of the long pile. (b) Distribution of peak axial force of the short pile.
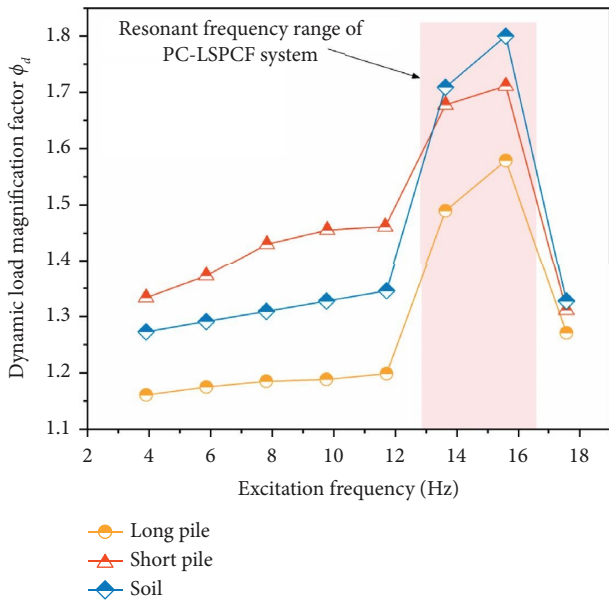

FIGURE 11: Relationships between the dynamic load magnification factor and the excitation frequency.

of composite foundation under different speed conditions, it can be seen that the train speed is negatively correlated with the cumulative settlement. The higher the train speed, the smaller the cumulative settlement, and the smaller the number of cycles of the N-S curve entering the gentle period.

In order to further study the relationship between the settlement S of composite foundation and the number of cycles N, the numerical fitting of the test results is carried out. The numerical fitting results show that the relationship between the settlement S of the composite foundation and the number of cycles N can be expressed by the following exponential function:

$$S = \alpha N^{\beta}, \qquad (4)$$

where α and β are the fitting parameters. Table 4 shows α, β, and the coefficient of determination R^2 obtained by numerical fitting, where R^2 is above 0.95, indicating that the reliability of numerical fitting results is high. It can be seen from Table 4 that with the increase of train speed, A increases and B decreases, indicating that the larger the train speed, the faster the initial development rate of settlement of a composite pile foundation, but the smaller is the number of cyclic loads entering the stable period of settlement.

4. Discussion

4.1. Spatial and Temporal Distribution of the PC-LSPCF Dynamic Response under Train Dynamic Load. From the analysis of the abovementioned test results, it can be seen that there is a certain correlation between the dynamic response of the PC-LSPCF under train dynamic load and the depth of foundation and the loading frequency (train speed). We draw the color mapping diagram of the peak acceleration response of the PC-LSPCF with depth and train speed. From Figures 13(a) and 13(b), it can be seen that the acceleration response peak of the PC-LSPCF is the smallest and the minimum value is 0.008 m/s² in the depth of 40–65 cm and the train speed of 80–160 km/h. The peak acceleration of PC-LSPCF is maximum in the interval of pile depth 0–40 cm and train speed 200–360 km/h with the maximum value 0.0502 m/s². The maximum acceleration response value in the actual project is 2.51 m/s² according to the similar ratio, which meets the design requirement of not more than 10 m/s² for roadbed vibration acceleration in China's "Technical Specification for Dynamic Acceptance of High-Speed Railway Projects." It shows that the PC-LSPCF has good
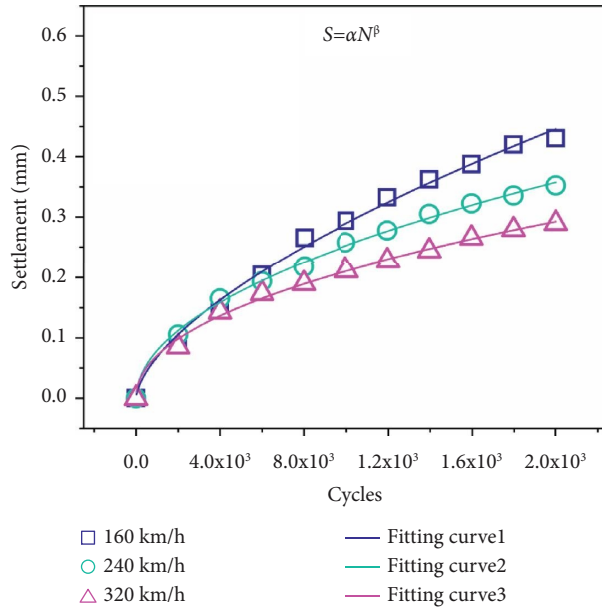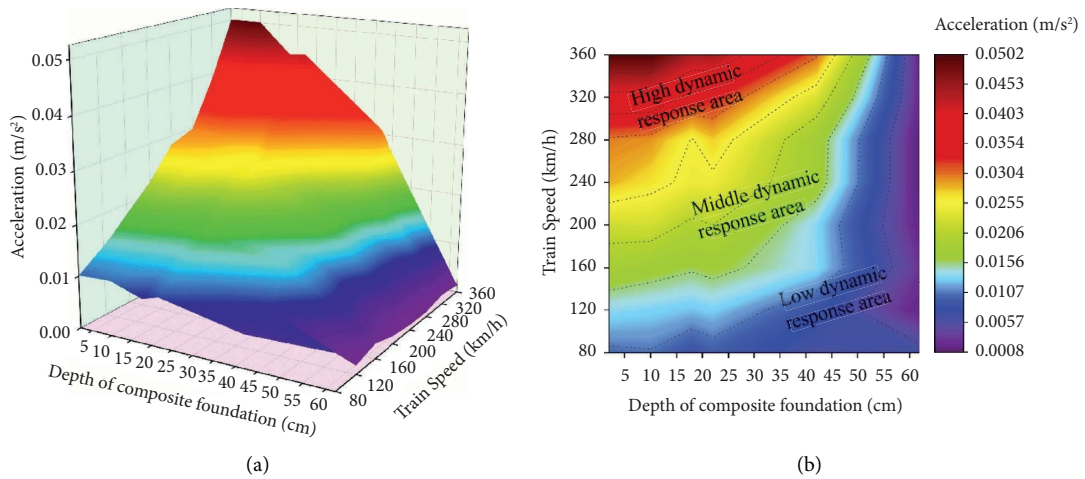
FIGURE 12: The cumulative settlement curve of PC-LSPCF.

(a)

(b)

$$A_{max} = -0.0039 + 533\exp\left\{-1/2\left(z - 15/30\right)^2 - 1/2\left(v - 4677/1006\right)^2\right\}, R^2 = 0.91$$
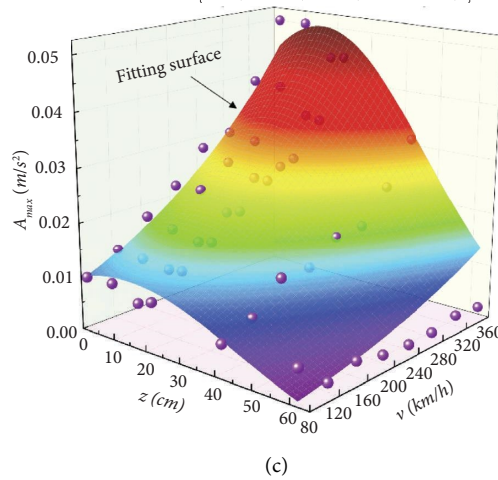

(c)

FIGURE 13: Temporal and spatial distribution of the acceleration response. (a) Three-dimensional surface mapping of the peak acceleration response of PC-LSPCF with velocity and depth. (b) The plane mapping of the peak acceleration response of PC-LSPCF with velocity and depth. (c) The fitting surface of the peak acceleration response distribution of PC-LSPCF.

TABLE 4: Fitting parameters.

Train speed (km/h)	α	β	R^2
160	2.98×10^{-4}	0.75	0.99
240	4.08×10^{-4}	0.70	0.98
320	6.07×10^{-4}	0.64	0.98

overall vibration resistance and is suitable for railway soft soil foundation treatment.

On the whole, the foundation depth is negatively correlated with the peak acceleration response of the PC-LSPCF, and the train speed is positively correlated with the peak acceleration response of the PC-LSPCF. As shown in Figure 13(c), in order to further clarify the relationship between PC-LSPCF acceleration response and foundation depth and train speed, Gauss2D surface fitting was performed on the acceleration response peak data of different depths of composite foundation under different speeds. The empirical equation is expressed as follows:

$$A_{\max} = -0.0039 + 533 \exp\left\{-\frac{1}{2}\left(\frac{z - 15}{30}\right)^2 - \frac{1}{2}\left(\frac{v - 4677}{1006}\right)^2\right\}, \quad (5)$$

where $A_{\max}$ is the peak acceleration response; z is the distance from the measuring point to the surface of composite foundation; and v is train speed.

Comparing 13(a) and 13(c), it can be seen that the fitting surface is basically consistent with the mapping surface of the real-side acceleration response data, and the correlation coefficient $R^2 = 0.91$ is close to 1, indicating that the fitting model is more realistic. It can be clearly seen from Figure 13(c) that the smaller the foundation depth z, the more prominent the dynamic response of PC-LSPCF, and the stronger the correlation with train speed v, while the dynamic response of the pile bottom at different speeds does not change significantly. From another point of view, with the increase in train speed, the influence depth range of train load on PC-LSPCF increases. According to the typical characteristics of the peak acceleration response, the peak acceleration response range of PC-LSPCF can be divided into three regions under the experimental conditions: $0 \text{ m/s}^2 < A_{\max} < 0.015 \text{ m/s}^2$ is defined as the low impact area, $0.015 \text{ m/s}^2 < A_{\max} < 0.030 \text{ m/s}^2$ is defined as the moderate impact area, and $0.030 \text{ m/s}^2 < A_{\max} < 0.050 \text{ m/s}^2$ is defined as the high impact area. When the train speed $v < 120 \text{ km/h}$ or the foundation depth $z > 50 \text{ cm}$, the train load is not sensitive to the dynamic effect of PC-LSPCF and belongs to the low influence area. When the train speed is $120 \text{ km/h} < v < 240 \text{ km/h}$ or the foundation depth $z < 50 \text{ cm}$, the train speed has a great correlation with the dynamic response of PC-LSPCF, and the peak class growth of the acceleration response is significant, which belongs to the moderate influence area. When the train speed $v > 240 \text{ km/h}$ or the foundation depth $z < 40 \text{ cm}$, the PC-LSPCF has a more severe dynamic response under the action of the train. The acceleration response of the 3/5 pile length below the pile top is severe, which is a height-affected zone. This result is similar to the results obtained by Bian et al. [28]. It should be noted that Figure 13(c) and the previous fitting

formula are only used in similar cases, and further research is needed to determine the application under other foundation conditions.

4.2. Deformation Evolution Characteristics of PC-LSPCF under Long-Term Vibration Load. Through the analysis of the test results, it is found that the dynamic stress of the pile, the dynamic stress of the soil, and the cumulative settlement trend of the composite foundation are similar. Considering the normalization of the measured data, the data are dimensionless. The abscissa is the number of dynamic load cycles, and the ordinate has its own meaning. Through multidata normalization processing, the correlation between data changes can be more intuitively expressed, and the response of PC-LSPCF under long-term dynamic load excitation can be obtained.

In order to make each sensor's data dimensionless, the pile dynamic stress, soil dynamic stress, and cumulative settlement of the composite foundation are normalized. The normalization formula is as follows:

$$X_{norm} = \frac{X - X_{\min}}{X_{\max} - X_{\min}}, \quad (6)$$

where X_{norm} is the normalized ordinate value; X is the measured value of each sensor; $X_{\max}$ is the maximum value of each sensor measured; and $X_{\min}$ is the minimum measured value of each sensor.

The normalized processing result is shown in Figure 14(a). It can be seen that there is a highly similar trend between the normalized pile dynamic stress and the soil dynamic stress. According to the stage change characteristics of dynamic stress, it can be divided into three stages: the rapid growth stage, the transitional growth stage, and the stable stage. Under the cyclic loading of small cycles, the stress on the pile and soil will increase rapidly. After a certain cycle, the stress on the pile and soil will increase slowly and finally remain stable. The normalized cumulative settlement also has a similar change trend, but the number of times the settlement deformation enters the stable period is much larger than that of the dynamic stress stable period, indicating that the settlement deformation of the long and short pile composite foundation has a " lag effect" relative to the change of dynamic stress. Through the dynamic stress distribution of long pile top, short pile top, and surface soil, the load sharing relationship of the pile and soil in long-short pile composite foundation can be obtained. Figures 14(b) and 14(c) show the load sharing ratio of the long pile, short pile, and soil under different vibration times. It can be seen that under the small cycle of train load, the load percentage of the long pile, short pile, and soil is not much different, and the role of the pile body is fully exerted.

(a)   (b)
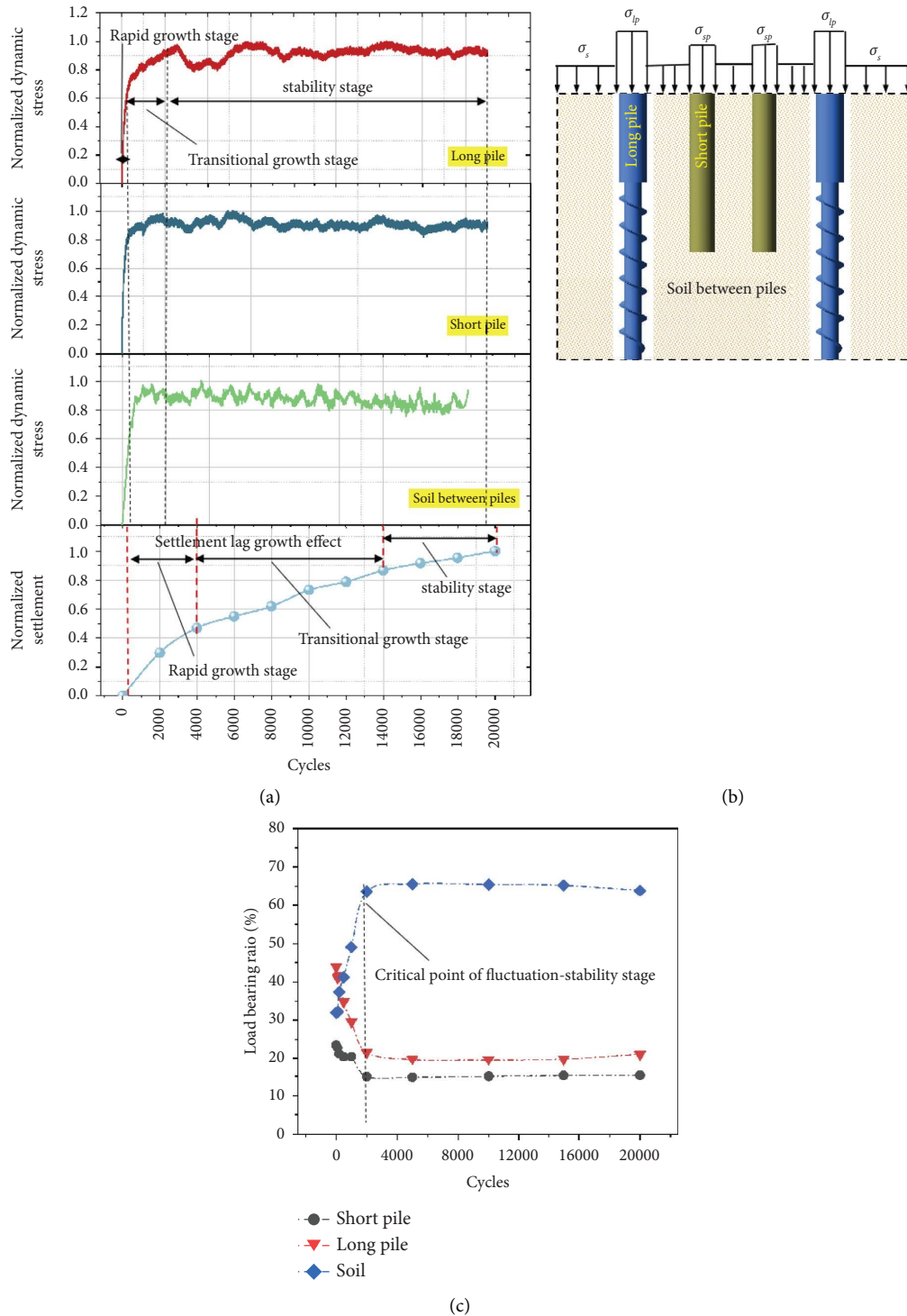

(c)

Figure 14: Stress deformation evolution of PC-LSPCF. (a) Normalized comparison of multiple source data. (b) Stress distribution for PC-LSPCF. (c) Load-bearing percentage of PC-LSPCF.

With the increase of vibration times, the load sharing relationship between the long pile, short pile, and soil is redistributed, the load bearing ratio of the soil increases, and the load bearing ratio of the pile decreases. Finally, after the vibration times are greater than 2000 times, the load sharing ratio of the composite foundation is expressed as soil > long pile > short pile, and the long pile-short pile-soil interaction remains stable in the long term.

5. Conclusion

In order to explore the dynamic characteristics and deformation characteristics of railway PC-LSPCF under long-term train load, we tested the dynamic characteristics of long piles, short piles, and soil between piles under long-term train load through an indoor dynamic model test. The dynamic amplification of the pile and soil under dynamic load and the temporal and spatial distribution of the peak response are analyzed, and the development mechanism of stress and deformation of PC-LSPCF under cyclic loading of large-cycle trains is revealed. The main findings are as follows:

(1) The axial force of long and short piles increases first and then decreases along the pile. The neutral point of the long pile is at 1/2 of the pile length, and the neutral point of the short pile is at 3/8 of the pile length.

(2) The resonance frequency of the long-short pile composite foundation system under train load is in the range of 14–16 Hz, and the sensitivity of the pile to dynamic load is greater than that of the surrounding soil.

(3) The train speed is negatively correlated with the cumulative settlement of PC-LSPCF. The higher the train speed, the smaller the cumulative settlement, and the smaller the number of cycles of the N-S curve entering the gentle period.

(4) The deformation of PC-LSPCF under long-term train loads can be divided into three stages: the extreme growth stage, the transitional growth stage, and the stable stage.

(5) With the increase in the number of train cyclic loads, the load sharing relationship between long piles, short piles, and soil will be redistributed, the load bearing ratio of soil will increase, the load bearing ratio of piles will decrease, and the load bearing relationship will remain stable for a long time after the vibration times are greater than 2000.

Data Availability

The data used to support the findings of this study are available from the corresponding author upon request.

Conflicts of Interest

The authors declare that they have no conflicts of interest.

Authors' Contributions

Wei Guan contributed equally to this work.

Acknowledgments

References

[1] Z. Sihua and N. Chen, "Long-short pile composite foundation strengthening technique in the application of the foundation treatment," in *Proceedings of the Shanghai International Conference on Technology of Architecture and Structure(ICTAS2009)*, pp. 332–337, Shanghai, China, June 2009.

[2] C. Longzhu, L. Fayun, H. Dazhi, and W. Guocai, "Field test study on application of long - short pile composite foundation in high-rise buildings," *Journal of Geotechnical Engineering*, vol. 2, pp. 167–171, 2004.

[3] X. Xinyu, Y. Xiangru, S. Shangwei, and Z. Xiangrong, "Analysis on properties of rigid and flexible long - short pile composite foundation," *Rock and Soil Mechanics*, vol. 5, pp. 877–882, 2007.

[4] J. Xu, X. Xu, and W. Yao, "New calculation method for the settlement of long-short-pile composite foundation based on virtual soil-pile model," *Arabian Journal of Geosciences*, vol. 15, no. 9, pp. 870–916, 2022.

[5] T. Niu, H. Liu, X. Ding, and C. Zheng, "Model tests on XCC-piled embankment under dynamic train load of high-speed railways," *Earthquake Engineering and Engineering Vibration*, vol. 17, no. 3, pp. 581–594, 2018.

[6] P.-N. Thach, H.-L. Liu, and G.-Q. Kong, "Vibration analysis of pile-supported embankments under high-speed train passage," *Soil Dynamics and Earthquake Engineering*, vol. 55, pp. 92–99, 2013.

[7] C. Zhang and G. Jiang, "Full-scale model testing of the dynamic response of lime-stabilized weathered red mudstone subgrade under railway excitation," *Soil Dynamics and Earthquake Engineering*, vol. 130, Article ID 105999, 2020.

[8] M. Ji, Z. Donggang, Z. Zhen, and Y. Mingli, "Design and calculation of long-short pile composite foundation," *Geotechnical engineering technology*, vol. 2, pp. 86–91, 2001.

[9] Y. Junlong, G. Xiaonan, and S. Bangchen, "Discussion on settlement calculation method of long-short pile composite foundation," *Building structure*, vol. 7, pp. 8–10+26, 2002.

[10] G. Xinsheng, G. Xiaonan, and Z. Xianming, "Discussion on design calculation method of long-short piles composite foundation," *Building structure*, vol. 7, pp. 3-4+7, 2002.

[11] D. Chao and G. Xiaonan, "Application of long-short pile composite foundation in high-rise buildings," *Building and Construction*, vol. 1, pp. 18–20, 2003.

[12] M.-h. zhao, Z. ling, and M.-h. Yang, "Settlement calculation of composite foundation with long and short piles based on shear displacement method," *Chinese Journal of Geotechnical Engineering*, vol. 9, pp. 994–998, 2005.

[13] S. B. Qian and L. H. Zhang, "Research of deformation characteristics of long-short pile composite foundation under rigid foundation," *Applied Mechanics and Materials*, vol. 638-640, pp. 694–698, 2014.

[14] Y. Guo, C. Lv, S. Hou, and Y. Liu, "Experimental study on the pile-soil synergistic mechanism of composite foundation with rigid long and short piles," *Mathematical Problems in Engineering*, vol. 2021, Article ID 6657116, pp. 1–15, 2021.

[15] W. Liu, X. Yang, S. Zhang, X. Kong, and W. Chen, "Analysis of deformation characteristics of long-short pile composite foundation in salt lake area, Iran," *Advances in Civil Engineering*, vol. 2019, Article ID 5976540, pp. 1–15, 2019.

[16] Y. Yang and J. Zhang, "Analysis of features of long and short pile composite foundation in high-rise buildings," *Soil*

Mechanics and Foundation Engineering, vol. 59, no. 1, pp. 92–101, 2022.

[17] D. Jihui, L. Fengran, D. chardonnay, and G.-q. ma, "Analysis of dynamic characteristics of composite foundation with cement-soil and CFG pile," *Comprehensive utilization of fly ash*, vol. 6, pp. 37–40, 2008.

[18] M. Y. Fattah, B. S. Zbar, and F. S. Mustafa, "Effect of soil saturation on load transfer in a pile excited by pure vertical vibration," *Proceedings of the Institution of Civil Engineers-Structures and Buildings*, vol. 174, no. 2, pp. 132–144, 2021.

[19] Y. Yiguo, K.-f. liu, and X.-y. xie, "Experimental study on deformation of long and short pile net composite foundation under cyclic load," *Journal of Zhejiang University*, vol. 55, no. 6, pp. 1027–1035, 2021.

[20] S. Xiao, J. Zhou, and Y. Tang, "Centrifuge model test on the behavior of geosynthetic-reinforced pile foundations under simulated train loads," *Acta Geotechnica*, vol. 17, no. 9, pp. 4131–4144, 2022.

[21] K. Liu, Y. Yang, L. Wang, J. Xu, and X. Xie, "Experimental investigation of geosynthetic-reinforced pile-supported composite foundations under cyclic loading," *Advances in Civil Engineering*, vol. 2020, pp. 1–11, Article ID 8886131, 2020.

[22] A. Al Shaer, D. Duhamel, K. Sab, G. Forêt, and L. Schmitt, "Experimental settlement and dynamic behavior of a portion of ballasted railway track under high speed trains," *Journal of Sound and Vibration*, vol. 316, no. 1-5, pp. 211–233, 2008.

[23] Y. Longcai, G. Qinghai, Z. Shunhua, W. Binglong, and G. Qiang, "Dynamic behaviors of pile foundation of high-speed railway bridge under long-term cyclic loading in soft soil," *Chinese Journal of Rock Mechanics and Engineering*, vol. 13, pp. 2362–2368, 2005.

[24] S. Guangchao, J.-l. li, S. K. Gang, R. Jas, W. Lehua, and H.-f. deng, "Model test on dynamic response of X-shaped pile-raft composite foundation for ballastless track under long-term train load," *Chinese Journal of Geotechnical Engineering*, vol. 44, no. 5, pp. 961–969, 2022.

[25] C. Renpeng, W. Zuozhou, J. Hongguang, and B. Xuecheng, "Experimental study of dynamic load magnification factor for type I track-subgrade system," *Rock and Soil Mechanics*, vol. 34, no. 4, pp. 1045–1052, 2013.

[26] Ministry of Railways Third Survey and Design Group Co Ltd, "China railway fourth survey and design institute Co., LTD. China academy of railway sciences," *TB 10621-2009 Code for Design of High-Speed Railway*, China Railway Publishing House, China, 2014.

[27] X. Bian, H. Jiang, and Y. Chen, "Accumulative deformation in railway track induced by high-speed traffic loading of the trains," *Earthquake Engineering and Engineering Vibration*, vol. 9, no. 3, pp. 319–326, 2010.

[28] X. Bian, H. Jiang, C. Cheng, Y. Chen, R. Chen, and J. Jiang, "Full-scale model testing on a ballastless high-speed railway under simulated train moving loads," *Soil Dynamics and Earthquake Engineering*, vol. 66, pp. 368–384, 2014.